Electronic Aspects of the Ferromagnetic Transition in Manganese Perovskites

J.-H. Park,[1] C. T. Chen,[1] S-W. Cheong,[1] W. Bao,[1,*] G. Meigs,[1] V. Chakarian,[2] and Y. U. Idzerda[2]
[1]*AT&T Bell Laboratories, 600 Mountain Avenue, Murray Hill, New Jersey 07974*
[2]*Naval Research Laboratory, Code 6345, Washington, D.C. 20375*
(Received 27 July 1995)

We have investigated the electronic structure associated with the ferromagnetic transition of $La_{1-x}Ca_xMnO_3$ and $La_{1-x}Pb_xMnO_3$ using high resolution photoemission, Mn $2p$ resonant photoemission, and O $1s$ x-ray absorption spectroscopies. The data clearly show that the band gap collapses below the Curie temperature (T_C) and the density of states at the Fermi level increases with cooling, providing a conclusive microscopic evidence for an insulator-metal transition. Our results suggest that strong small polaron effects, which contribute to a charge fluctuation energy of $\sim$1.5 eV, are responsible for the insulating behavior above T_C which has been enigmatic in the double-exchange model. [S0031-9007(96)00255-4]

PACS numbers: 71.30.+h, 72.80.Ga, 78.70.Dm, 79.60.Bm

The discovery of colossal magnetoresistance in mixed-valent manganese perovskites, such as $La_{1-x}Ca_xMnO_3$ and $La_{1-x}Pb_xMnO_3$, has attracted renewed interest in these systems, especially due to their potential technological applications [1–6]. The undoped compound ($x = 0$) is an antiferromagnetic insulator, commonly observed in many transition metal oxides, while the system with a nominal doping ($0.2 \lesssim x \lesssim 0.5$) undergoes a paramagnetic to ferromagnetic (PF) transition upon cooling [7,8]. Since the transition is accompanied by a large decrease in resistance, it has often been referred to as a metal to insulator (MI) transition. This behavior has traditionally been explained with the double-exchange model proposed in the 1950s [9], and the resistivity decrease has been considered as a mobility increase by spin ordering in the ferromagnetic state. However, the insulatorlike high resistivity above the transition temperature T_C has been enigmatic in the model, and, furthermore, lack of detailed spectroscopic studies limits the microscopic understanding of the PF transition.

Doped manganese perovskites are mixed-valent systems containing Mn^{3+} ($3d^4$) and Mn^{4+} ($3d^3$) ions. Under the circumstance of the octahedral symmetry of the Mn sites, the configurations become $t_{2g}^3 e_g^1(^5E)$ for the Mn^{3+} and $t_{2g}^3(^4A_2)$ for the Mn^{3+}. In the double-exchange model, the e_g electrons are treated as mobile charge carriers interacting with the Mn^{4+} ($S = 3/2$) background. The carrier hopping depends on the relative alignment of the carrier spin to the localized Mn^{4+} spin. When the two spins are aligned, the carrier avoids the strong on-site Hund exchange energy, and thus hops easily [9]. Theoretical calculations for the transport properties based on this model have shown qualitative agreements with the experimental data [2,10]. However, due to the partially filled e_g orbital, the system is expected to be *always* metallic, and the double-exchange model considering primarily the spin-dependent electron hopping mechanism turns out to be not enough to explain the insulatorlike behavior above T_C. Thus it was speculated that some additional effects, such as the Jahn–Teller-type polaron effect, to the double-exchange model are needed to reduce the carrier hopping substantially [3].

In this Letter, we report high resolution photoemission spectroscopy (PES), O $1s$ x-ray absorption spectroscopy (XAS), and Mn $2p$ resonant photoemission spectroscopy (RPES) studies on $La_{1-x}Ca_xMnO_3$ and $La_{1-x}Pb_xMnO_3$. The data show that the band gap collapses below T_C, providing a conclusive microscopic evidence for an MI transition. The detailed studies of $La_{1-x}Ca_xMnO_3$ with various Ca concentrations show that strong small polaron effects, which contribute to a charge fluctuation energy of $\sim$1.5 eV for $Mn^{3+} + Mn^{4+} \rightarrow Mn^{4+} + Mn^{3+}$, are responsible for the insulating behavior above T_C.

Polycrystalline $La_{1-x}Ca_xMnO_3$ samples with various Ca concentrations and a $La_{0.7}Pb_{0.3}MnO_3$ single crystal were prepared by standard solid-state reaction and the flux method, respectively, and the measurements were performed at the AT&T Bell Laboratories Dragon beam line at the National Synchrotron Light Source (NSLS) [11]. All the samples, except for the $LaMnO_3$, were oxygen stoichiometric [8] and x-ray powder diffraction measurements showed single-phase patterns. The as-grown $LaMnO_{3+\delta}$ ($\delta \approx 0.1$) sample was annealed in Ar atmosphere, reducing δ down to $\sim$0.03.

For a doping-dependent study of $La_{1-x}Ca_xMnO_3$, the samples were scraped at 280 K with diamond files in a vacuum better than 1.5×10^{-10} torr. For temperature-dependent measurements of $La_{0.67}Ca_{0.33}MnO_3$ and $La_{0.7}Pb_{0.3}MnO_3$, the samples were cleaved *in situ* and the temperature was controlled within 1 K. The cleaned surfaces were found to last for 3 to 5 h, as confirmed by the absence of O $1s$ satellite and 9 eV binding energy peaks in PES spectra taken at 700 and 110 eV photon energies, respectively. These two peaks are known to appear with surface contamination [5]. To keep the cleanliness of the surface, the samples were scraped or cleaved several times, and all measurements were repeated to ensure reproducibility of data. The binding

energies of PES spectra were referred to the chemical potential of a clean Pt that is in electrical and thermal contact with the samples.

Figure 1 shows the doping dependent spectra of $La_{1-x}Ca_xMnO_3$ in the paramagnetic phase taken at 280 K. The PES spectra were taken at 500 eV photon energy and with overall experimental resolution of 0.6 eV. The XAS spectra were obtained by using the total electron yield method with a photon energy resolution of 0.15 eV. The PES spectra in Fig. 1(a) display the valence band as well as Ca $3p$, O $2s$, and La $5p$ shallow core levels as labeled in the figure. These spectra were normalized to give the same O $2s$ peak height. All three core levels were found to shift, by the same amount, toward lower binding energy with increasing Ca concentration. This reflects a monotonic chemical-potential shift with Ca concentration as summarized in the inset [12].

To investigate the effects on the electronic structure by Ca doping, the valence band spectra are replotted in Fig. 1(b) after the chemical-potential shift is compensated so that the core levels are aligned. At this photon energy, the O $2p$ contribution is comparable to the Mn $3d$ one [13]. A significant intensity is observed between 0.0 and 1.5 eV in $x = 0$ ($LaMnO_3$, Mn^{3+}) spectrum. The intensity decreases systematically with increasing Ca content, and vanishes completely in $x = 1$ ($CaMnO_3$, Mn^{4+}) spectrum. For energies greater than 1.5 eV, both the valence band and core-level regions show systematic change as a function of x. It is intriguing that the spectrum of a given x can be approximated to a weighted average of the $x = 0$ and 1 spectra. Figure 1(c) shows an example for the $x = 0.48$ spectrum, in which the solid curve is the sum of 52% of the $x = 0$ spectrum and 48% of the $x = 1$ spectrum. The averaged spectrum is almost identical to the $x = 0.48$ spectrum, except for a small difference in the peak width of Ca $3p$ (nevertheless, the area is conserved).

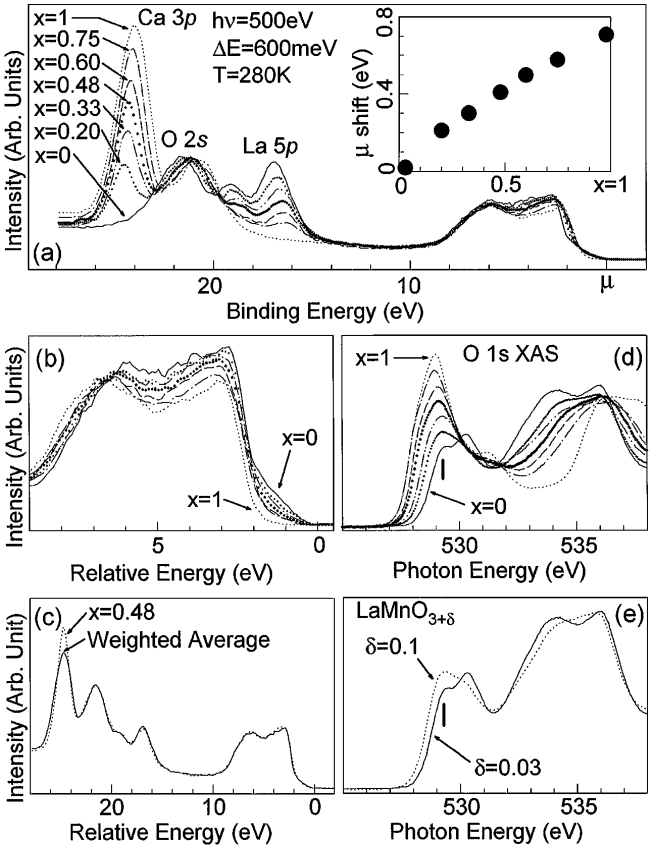

FIG. 1. Doping-dependent PES and O $1s$ XAS spectra of $La_{1-x}Ca_xMnO_3$ as described in the text. (a) Valence band and shallow core level, Ca $3p$, O $2s$, and La $5p$, PES spectra. The chemical-potential shifts are summarized in the inset. (b) Valence band PES after the chemical-potential shifts are compensated. (c) The PES spectrum of the $x = 0.48$ sample is compared with the weighted average of the $x = 1$ and the $x = 0$ spectra, i.e., 52% ($x = 0$) + 48% ($x = 1$). (d),(e) O $1s$ XAS spectra.

A systematic spectral change with x is also observed in the O $1s$ XAS spectra as presented in Fig. 1(d). Because of core hole effects, some spectral weight transfers to lower energy states, but the spectrum of the doped sample can still be understood as a linear combination of the $x = 0$ and the $x = 1$ as discussed in the O $1s$ XAS study of $La_{1-x}Sr_xMnO_3$ [14]. We note that the shoulder of the $x = 0$ spectrum (indicated by a vertical line) is not intrinsic to $LaMnO_3$ but due to excess oxygen which introduces Mn^{4+} as Ca dopant does. It is supported by the intensity decrease of the shoulder with decreasing excess oxygen as is clearly seen in the XAS spectra of as-grown ($\delta = 0.1$) and Ar-annealed ($\delta = 0.03$) $LaMnO_{3+\delta}$ samples in Fig. 1(e) [15].

Figure 2 shows one electron removal ($N \rightarrow N - 1$) and addition ($N \rightarrow N + 1$) spectra of $LaMnO_3$ and of $CaMnO_3$. Although the O $1s$ XAS spectra are not ideal for representing the $N + 1$ spectra due to core hole effects, they do provide a reasonable approximation [16]. The O $1s$ XAS spectra are shifted so that the main features of the $LaMnO_3$ spectrum are aligned with its inverse photoemission spectrum [4]. The rather complicated spectral shape in the valence band can be understood by the many-body approach using the Anderson impurity Hamiltonian as has been demonstrated for other transition metal oxides [17]. We will focus here, however, on the lowest energy excitation states, which are most relevant to the electrical and magnetic properties, also the related model Hamiltonians including the double-exchange model. The lowest energy $N - 1$ state, the ground state, and the lowest energy $N + 1$ state of $CaMnO_3$ (Mn^{4+}) have $t_{2g}^2(^3T_1)$, $t_{2g}^3(^4A_2)$, and $t_{2g}^3e_g^1(^5E)$ symmetries, and the corresponding states of $LaMnO_3$ (Mn^{3+}) have $t_{2g}^3(^4A_2)$, $t_{2g}^3e_g^1(^5E)$, and $t_{2g}^3e_g^2(^6A_1)$ symmetries, respectively. The lowest energy $N - 1$ and $N + 1$ states of both systems are indicated in the figure. The lowest $N + 1$ state of $CaMnO_3$ appears as a shoulder in the XAS spectra, because it is obscured by a higher energy state of a $t_{2g}^4(^3T_1)$ symmetry. As explained above, the 1 eV shoulder in the XAS spectra of $LaMnO_3$ is not intrinsic, and, therefore, the 2 eV peak is its lowest energy

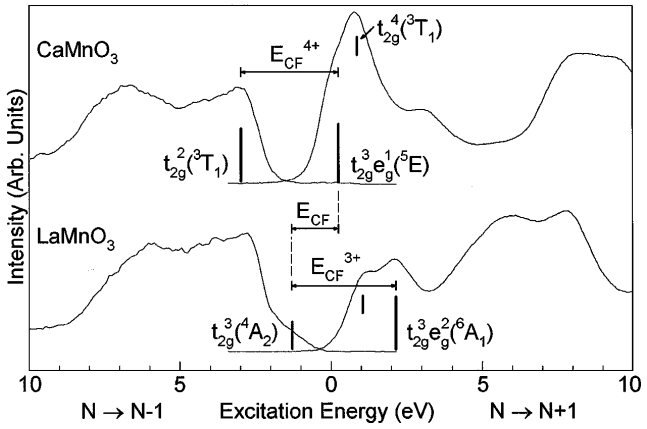

FIG. 2. One electron removal, $N \rightarrow N-1$, and addition, $N \rightarrow N+1$, excitation spectra as described in the text.

$N+1$ state. The energy separations between the lowest energy $N-1$ and $N+1$ peaks of $CaMnO_3$ and of $LaMnO_3$ were estimated to be $E_{CF}^{4+} = 3.2 \pm 0.4$ eV and $E_{CF}^{3+} = 3.4 \pm 0.4$ eV, respectively. According to a recent many-body analysis for other transition metal oxides, these energy separations are attributed to the smaller energy of the O $2p$ to Mn $3d$ charge transfer energy, Δ, and the on-site d-d Coulomb energy, U [18]. For $CaMnO_3$, Δ is 3.0 ± 0.5 eV as estimated from our O $1s$ RPES data [19] and U is 5.2 ± 0.3 eV as calculated from the Racha parameters of MnO [20]. Using the same methods, Δ and U of $LaMnO_3$ were estimated to be 4.5 ± 0.5 eV and 3.5 ± 0.3 eV, respectively, which are comparable to those deduced from Mn $2p$ photoemission analysis [4]. Therefore, E_{CF}^{4+} of $CaMnO_3$ is associated with the smaller energy Δ, and E_{CF}^{3+} of $LaMnO_3$ is associated with the smaller energy U, consistent with the findings, $E_{CF}^{4+} \approx \Delta$ and $E_{CF}^{3+} \approx U$ [21].

For the mixed valent system $La_{1-x}Ca_xMnO_3$ with $0 < x < 1$, which can be described electronically by a linear combination of $LaMnO_3$ and $CaMnO_3$ as demonstrated in Fig. 1, E_{CF} is 1.5 ± 0.4 eV as estimated from the energy separation between the $t_{2g}^3 e_g^1(^5E)$ state of $CaMnO_3$ and the $t_{2g}^3(^4A_2)$ state of $LaMnO_3$. This E_{CF} corresponds to the energy for the $t_{2g}^3 e_g^1(Mn^{3+}\ \text{site}) + t_{2g}^3(Mn^{4+}\ \text{site}) \rightarrow t_{2g}^3(Mn^{3+}\ \text{site}) + t_{2g}^3 e_g^1(Mn^{4+}\ \text{site})$ charge fluctuation process, which is supposed to vanish in the double-exchange model. The observed finite E_{CF} suggests a strong polaron effect due to localization of e_g electrons. The localization, which can be attributed to the random distribution of Ca^{2+} incorporating with the strong correlation effect of Mn $3d$ electrons, causes local lattice distortions, the so called "small polarons," and contributes the difference, E_{CF}, in potential at Mn^{3+} and Mn^{4+} sites. This small polaron, which has been discussed in the Anderson localization [22], is induced from a large difference ($\sim 20\%$) in the ionic size of Mn^{3+} and Mn^{4+} (6%–7% difference in Mn-O distance) [23], and should be distinguished from the Jahn–Teller-type polaron, proposed recently [3], which results from tetragonal distortions of MnO_6 octahedra to lower the Mn^{3+} ($t_{2g}^3 e_g^1$) energy. Considering the disappearing temperature ($\sim$700 K) of the Jahn–Teller-type lattice distortion in $LaMnO_3$, the Jahn-Teller distortion is expected to contribute at most a few tenths of an eV which is much smaller than the observed E_{CF}. Hence, the charge fluctuation energy E_{CF}, which is responsible for the low conductivity above T_C, should be understood by the strong small polaron effects including a minor contribution of the Jahn-Teller distortion. The fact, furthermore, that the system with $0 < x < 1$ can be approximated electronically to a linear superposition of $x = 0$ and 1 provides the spectroscopic evidence for the strong small polaron effects in this system.

To study the electronic change accompanied by the ferromagnetic transitions in $La_{0.67}Ca_{0.33}MnO_3$ ($T_C \approx$ 260 K) and in $La_{0.7}Pb_{0.3}MnO_3$ ($T_C \approx 330$ K), we have measured their high resolution PES and Mn $2p$ RPES spectra at various temperatures. The high resolution and on-resonance spectra were taken at 110 and 642 eV photon energies with 0.06 and 0.6 eV resolutions, respectively. Because of the limitation of our temperature controller, we were unable to raise the sample temperature beyond the T_C of $La_{0.7}Pb_{0.3}MnO_3$. Figure 3(a) shows the high resolution wide-scan PES spectra of both samples, exhibiting nearly no difference between the two extreme temperatures, except for a minor chemical-potential shift of $\sim$70 meV and an intensity variation near the Fermi level. The magnified spectra near the Fermi level are shown in Fig. 3(b). For $La_{0.67}Ca_{0.33}MnO_3$, no density of states at the Fermi level $n(\varepsilon_F)$ is observed in the 280 K spectrum, but $n(\varepsilon_F)$ increases upon cooling below T_C and a metallic Fermi edge is clearly observed in the 80 K spectrum. A similar temperature dependence was also observed in $La_{0.7}Pb_{0.3}MnO_3$. These results provide conclusively that the ferromagnetic transition is accompanied by an MI transition, which causes the large resistivity change near T_C, and the high resistivity above T_C is not due to the mobility reduction by spin disorder but due to the disappearance of density of states at E_F. Furthermore, the gradual appearance of $n(\varepsilon_F)$ upon cooling is also consistent with the resistivity behavior showing no discontinuity near T_C as well as the considerable decrease even well below T_C [8].

Although the MI transition at E_F was clearly observed in the 110 eV high resolution spectrum, the temperature dependence of the Mn $3d$ states is not conclusive due to the O $2p$ states which have 2 times larger intensity at this photon energy [13]. The obscured Mn $3d$ states can be explored through the Mn $2p$ RPES process, $3d^n \rightarrow \underline{c}3d^{n+1} \rightarrow 3d^{n-1} + e^-$, where $\underline{c}$ is a Mn $2p$ hole. The Mn $3d$ states are enhanced by more than 20 times and thus completely dominate the valence band spectrum at the on-resonance. Figure 3(c) shows the on-resonance spectra of both compounds, which exhibit clearly two $3d$-removal states. One locates at $\sim$2.5 eV binding energy with $t_{2g}^2 e_g^1(^4T_2)$ symmetry and the other at $\sim$1 eV with

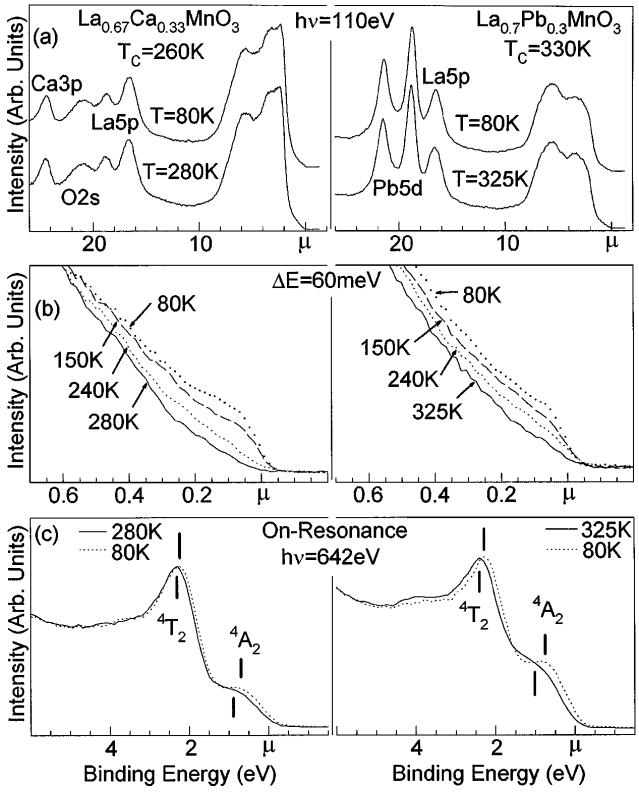

FIG. 3. Temperature dependent PES spectra of $La_{0.67}Ca_{0.33}MnO_3$ (left panel) and $La_{0.7}Pb_{0.3}MnO_3$ (right panel). The $h\nu = 110$ eV high resolution spectra for (a) wide scan and for (b) near E_F region. (c) Mn $2p_{3/2}$ edge on-resonant spectra.

$t_{2g}^3(^4A_2)$ symmetry. Upon cooling from the high to the low temperature, the $^4T_2$ and $^4A_2$ states shift to low binding energy, and the energy shifts were estimated $\sim$0.1 and $\sim$0.2 eV ($\sim$0.15 and $\sim$0.25 eV) from line shape analysis for $La_{0.67}Ca_{0.33}MnO_3$ ($La_{0.7}Pb_{0.3}MnO_3$), respectively [19]. For both samples, the $^4A_2$ peaks become more observable at the low temperature, partially due to their larger energy shifts as compared to those of $^4T_2$ states. This energy shift of the $^4A_2$ state indicates that the E_{CF} discussed above is reduced upon cooling, consistent with the band gap closing and $n(\varepsilon_F)$ increasing observed in the high resolution data.

According to the double-exchange model, the hopping energy of the e_g electron carrier depends significantly on the relative alignment of the spins of Mn ions. At $T > T_C$, the hopping energy is insufficient to overcome the charge fluctuation energy (E_{CF}) and hence the system is in the insulating phase. At $T < T_C$, the spins of Mn ions start to align ferromagnetically, enhancing the hopping energy. This increase in hopping energy may affect the small polaron energy and the Jahn-Teller distortion, and reduces E_{CF}. The reduction in E_{CF} and the increase in hopping energy lead to the band gap closing and $n(\varepsilon_F)$ increasing upon cooling.

In conclusion, we, for the first time, report detailed spectroscopic data of colossal magnetoresistance compounds of doped manganese perovskites. The electronic structure of $La_{1-x}Ca_xMnO_3$ can be approximated to a linear superposition of $LaMnO_3$ and $CaMnO_3$, supporting the strong small polaron effects. The high resolution data demonstrate the insulator-metal transition near the Curie temperature. The strong small polaron effects, which contribute to the charge fluctuation energy E_{CF} together with the Jahn-Teller distortion, need to be incorporated into the double-exchange model for understanding the fascinating electronic and magnetic transition, i.e., the PI-FM transition.

We thank B. I. Shraiman for helpful discussions. The NSLS is supported by the DOE under Contract No. DE-AC02-76CH00016.

*Permanent address: Department of Physics, Johns Hopkins University, Baltimore, MD 21218.

[1] C. W. Searle and S. T. Wang, Can. J. Phys. **47**, 2703 (1969); K. Chabara *et al.*, Appl. Phys. Lett. **63**, 1990 (1993); S. Jin *et al.*, Science **264**, 413 (1994).
[2] N. Furukawa, J. Phys. Soc. Jpn. **63**, 3214 (1994); Y. Tokura *et al.*, J. Phys. Soc. Jpn. **63**, 3931 (1994).
[3] A. J. Millis *et al.*, Phys. Rev. Lett. **74**, 5144 (1995).
[4] A. Chainani *et al.*, Phys. Rev. B **47**, 15 397 (1993).
[5] T. Saitoh *et al.*, Phys. Rev. B **51**, 13 942 (1995).
[6] Y. Okimoto *et al.*, Phys. Rev. Lett. **75**, 109 (1995).
[7] G. H. Jonker and J. H. Van Santen, Physica (Utrecht) **16**, 337 (1950); E. O. Wollan and W. C. Koehler, Phys. Rev. **100**, 545 (1955).
[8] P. E. Schiffer *et al.*, Phys. Rev. Lett. **75**, 3336 (1995).
[9] C. Zener, Phys. Rev. **82**, 403 (1951); P. W. Anderson and H. Hasegawa, Phys. Rev. **100**, 675 (1955); J. Goodenough, Phys. Rev. **100**, 564 (1955); P.-G. de Gennes, Phys. Rev. **118**, 141 (1960).
[10] K. Kubo and N. Ohata, J. Phys. Soc. Jpn. **33**, 21 (1972).
[11] C. T. Chen, Nucl. Instrum. Methods. Phys. Res., Sect. A **256**, 595 (1987).
[12] The chemical potential might be affected by defect states in the insulating phase.
[13] J. J. Yeh and I. Lindau, At. Data Nucl. Data Tables **32**, 1 (1985).
[14] M. Abbate *et al.*, Phys. Rev. B **46**, 4511 (1992).
[15] In the 528–531 eV energy region, only one state, which corresponds to the $t_{2g}^3e_g^2(^6A_1)$ state, is also expected in the corresponding theoretical calculation for the O 1*s* XAS [16] spectrum.
[16] F. M. F. de Groot *et al.*, Phys. Rev. B **40**, 5459 (1989); J. van Elp *et al.*, Phys. Rev. B **44**, 6090 (1991).
[17] A. J. Fujimori and F. Minami, Phys. Rev. B **30**, 957 (1984); G. A. Sawatzky and J. W. Allen, Phys. Rev. Lett. **53**, 2339 (1984).
[18] J. Zaanen *et al.*, Phys. Rev. Lett. **55**, 418 (1985).
[19] J.-H. Park *et al.* (unpublished).
[20] J. van Elp *et al.*, Phys. Rev. B **44**, 1530 (1991).
[21] The small difference is due to Mn $3d-$O $2p$ hybridization, and turns out to be less than a few tenths of an eV in the cluster model calculations.
[22] N. F. Mott and E. A. Davis, *Electronic Process in Non-Crystalline Materials* (Clarendon Press, Oxford, 1979).
[23] R. D. Shannon and C. T. Prewitt, Acta Crystallogr. Sect. B **25**, 925 (1969).